Available online at www.sciencedirect.com

ScienceDirect

Acta Materialia 93 (2015) 12–23

Acta MATERIALIA

www.elsevier.com/locate/actamat

Crystal plasticity simulations using nearest neighbor orientation correlation function

V. Sundararaghavan,[a,*] A. Kumar[b] and S. Sun[c]

[a]*Aerospace Engineering, University of Michigan, Ann Arbor, MI, USA*
[b]*Oak Ridge National Lab, Oak Ridge, TN, USA*
[c]*Exmar Offshore, Houston, TX, USA*

Received 6 February 2015; revised 10 April 2015; accepted 10 April 2015
Available online 27 April 2015

Abstract—A probabilistic scheme is presented for simulating evolution of polycrystalline microstructures during deformation. Microstructure images are described using a compact descriptor called the nearest-neighbor conditional orientation correlation function, defined as the probability density of occurrence of a crystal orientation at one pixel distance from a known orientation. The neighborhood information obtained from this function is used to correct a Taylor-based formulation of crystal plasticity. A finite differencing scheme is developed to capture equilibrium of each orientation in an average sense. The predictions of textures and stresses using our approach are compared against crystal plasticity finite element model of a planar polycrystalline microstructure. We find that the new descriptor is able to capture texture components that are otherwise missed by the Taylor model and provides consistent improvements in the prediction of reorientation and stresses. The simulation speed is significantly faster than crystal plasticity finite element method and is more comparable to that of Taylor models.

Keywords: Plastic deformation; Texture; Finite element analysis; Simulation; Theory

1. Introduction

Integrated Computational Materials Engineering (ICME) [1] paradigm for metal-forming processes proposes stronger tie-in of microstructural models to engineering simulations. The microstructural model of choice for polycrystalline alloys is the crystal plasticity finite element method (CPFE) [2–6]. Here, mechanical properties of aggregates of grains are analyzed by discretizing the grains into finite elements and modeling texture development using crystal plasticity constitutive models. There are two primary issues when dealing with such an approach. Firstly, multiscale simulations that use finite element representation of the underlying microstructure are computationally prohibitive. Secondly, polycrystalline microstructures vary as a function of location in the raw material and compact representations are needed to model this variability.

An alternate class of schemes developed in recent years allow compact representation of microstructures using probabilistic descriptors. The simplest of these descriptors is the one-point probability measure, the orientation distribution function (ODF), which quantifies the volume fractions of crystals in the orientation space. Under an applied deformation, texturing is simulated by numerically evolving the ODF using conservation laws [7]. Conventional solution schemes are based upon representation of the ODF using a series of harmonics [8–10] or finite elements [11–13]. The ODF representation is extremely compact in comparison to discretized microstructures used in CPFE, leading to significant speed up in microstructure analysis. However, ODF representation does not contain information about the local neighborhood of crystals. Thus, equilibrium across grain boundaries cannot be captured and a Taylor assumption ([14], where all crystals deform identically) is used. Such a constraint leads to a stiff upper bound stress response, textures that are sharper than measured and texture components that cannot be captured [15].

The next level of descriptors, the two–point orientation correlation function (OCF), $\mathcal{F}(\boldsymbol{g}', \boldsymbol{g}, \boldsymbol{r})$, gives the probability density of finding orientations $\boldsymbol{g}'$ and $\boldsymbol{g}$ at the end points of a randomly placed vector $\boldsymbol{r}$ within the microstructure. This descriptor contains neighborhood information and holds the promise of modeling grain equilibrium, thereby relaxing the Taylor assumption. Representations of the OCF in the form of global approximations (exponentially decaying functions based on the Corson's model [16,17] and Fourier space representations [18]) and local approximations (based on finite elements, [19]) have been studied

* Corresponding author. Tel.: +1 734 615 7242; e-mail: veeras@umich.edu

http://dx.doi.org/10.1016/j.actamat.2015.04.016
1359-6462/

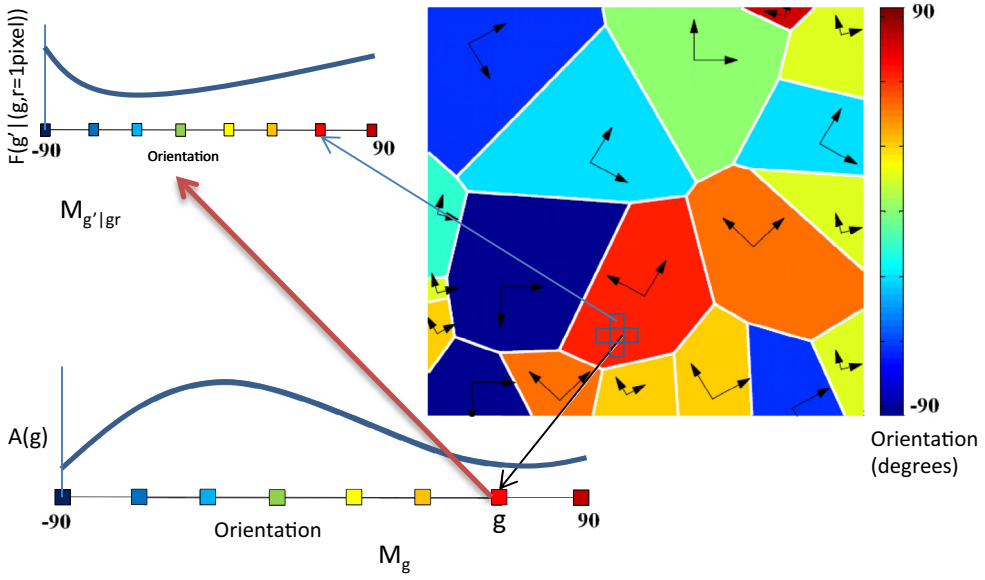

Fig. 1. NNOCF sampling from a microstructure (color coded based on grain orientation). The finite element mesh M_g represents the volume density of each orientation (color). The NNOCF mesh $M_{g'|gr}$ attached to a node g in mesh M_g represents orientation distribution for the nearest neighbor pixels of g. (For interpretation of the references to color in this figure legend, the reader is referred to the web version of this article.)

in the past. However, the two-point measure is high dimensional (e.g. OCF for a 3D FCC polycrystal is nine dimensional) and there is still a significant need for reduced representations.

Considerable improvements in OCF representation can be realized by including the physics of deformation processes. For example, in viscoplastic self consistent (VPSC) schemes, Green's function models the interaction between crystals [20,21]. The function decays with distance and can be used to estimate a cut-off radius beyond which correlation information is redundant [19]. However, this radius may encompass several grains and storage requirements are still significant. In this paper, we recognize that the nearest neighbor pixels (situated near the singularity of the Green's function) carry most of the grain interaction information. We explore the use of a conditional OCF ($\mathcal{F}(\boldsymbol{g}'|\boldsymbol{g},\boldsymbol{r})$) truncated to the nearest neighbors, hereafter called the nearest neighbor conditional orientation correlation function (NNOCF). The descriptor is extremely compact and we show that it can be used to locally enforce equilibrium (in an average sense) for each orientation using a novel finite differencing scheme. The present model significantly enhances the scope of our previous probabilistic model published in this journal [13], through addition of crystal neighborhood effects on texture development. The model is explained in Section 2. To show the relevance of this work to the material community, we have performed comparison of our new approach to verified crystal plasticity finite element codes of Refs. [13,22] in Section 3 and show testable predictions in cases where Taylor models fail and the use of two–point correlations resolves the problem. The discussion and conclusions are presented in Section 4.

2. Probabilistic representation

The complete orientation space of a polycrystal can be reduced to a smaller subset, called the fundamental region, as a consequence of crystal symmetries. Within the fundamental region, each crystal orientation is represented uniquely by a coordinate $\boldsymbol{g}$, the parametrization for the rotation (eg. Euler angles, Rodrigues vector [23]). The ODF, represented by $\mathcal{A}(\boldsymbol{g})$, describes the local density of crystals over the fundamental region. Consider a region R_δ which is a ball of radius δ centered at orientation $\boldsymbol{g}$ in the fundamental region. Let $v_f(R_\delta)$ be the volume fraction of crystals that have orientations that occur within volume R_δ. The ODF at an orientation $\boldsymbol{g}$ is defined as:

$$\mathcal{A}(\boldsymbol{g}) = \lim_{\delta\to 0} \frac{v_f(R_\delta)}{\int_{R_\delta} d\boldsymbol{g}} \tag{1}$$

The ODF is represented in this work over a finite element mesh (M_g) of the fundamental region. The ODF at any given orientation can be obtained by interpolating the nodal values of the element containing that orientation.

The nearest-neighbor conditional orientation correlation function (NNOCF), $\mathcal{F}(\boldsymbol{g}'|(\boldsymbol{g},\boldsymbol{r}))$, gives the probability density of occurrence of an orientation $\boldsymbol{g}'$ at the end point of a vector $\boldsymbol{r}$ (of one pixel length) emanating from a given orientation $\boldsymbol{g}$ (Fig. 1). The NNOCF is also represented in the FE discretized fundamental region (called mesh $M_{g'|gr}$, Fig. 1). In a 2D model of the microstructure (Fig. 1), four such meshes are needed at every node point in M_g corresponding to the four nearest neighbor pixels. The NNOCF satisfies the following conservation equations at all times during deformation[1]:

$$\begin{aligned} &\int \mathcal{F}(\boldsymbol{g}'|(\boldsymbol{g},\boldsymbol{r}))d\boldsymbol{g}' = 1, \mathcal{F}(\boldsymbol{g}'|(\boldsymbol{g},\boldsymbol{r})) \geqslant 0 \\ &\int \mathcal{A}(\boldsymbol{g}')d\boldsymbol{g}' = 1, \mathcal{A}(\boldsymbol{g}') \geqslant 0 \end{aligned} \tag{2}$$

In addition to the above constraints, the orientation space corresponding to all possible $\boldsymbol{g}$'s must satisfy the crystallographic symmetries of the chosen system (FCC,

[1] The OCF also satisfies the r-interdependence equation as described in [19]. However, due to lack of information beyond the nearest neighbors, such a constraint cannot be enforced in this work.

HCP, etc.) and the switching symmetry of the two–point measure, namely,

$$\mathcal{F}(\boldsymbol{g}|(\boldsymbol{g}',\boldsymbol{r}))\mathcal{P}(\boldsymbol{r}|\boldsymbol{g}')\mathcal{A}(\boldsymbol{g}') = \mathcal{F}(\boldsymbol{g}'|(\boldsymbol{g},\boldsymbol{r}))\mathcal{P}(\boldsymbol{r}|\boldsymbol{g})\mathcal{A}(\boldsymbol{g}) \tag{3}$$

Here, $\mathcal{P}(\boldsymbol{r}|\boldsymbol{g})$ gives the probability density of occurrence of vector $\boldsymbol{r}$ from a location with orientation $\boldsymbol{g}$, which accounts for the finite size of the sampled microstructure [19]. In this work, we simplify the analysis by assuming $\mathcal{P}(\boldsymbol{r}|\boldsymbol{g}') = \mathcal{P}(\boldsymbol{r}|\boldsymbol{g}) = \mathcal{P}(\boldsymbol{r})$.

2.1. Probability update in finite element spaces

The probabilities are evolved from time $t = 0$ from an initial NNOCF that satisfies the conservation equation (2). During deformation, the initial orientation $\boldsymbol{g}_o$ of a crystal reorients to a new orientation $\boldsymbol{g}_t$ at time t. We assume that the new orientation $\boldsymbol{g}_t$ can be computed using a crystal plasticity constitutive model (described later in Section 2.3). Our objective in this section is to compute the new ODF and NNOCF at time t. For this, the finite element mesh of fundamental region M_g is deformed, with nodes located at $\boldsymbol{g}_o$ moved to new locations $\boldsymbol{g}_t$. The ODF $\mathcal{A}(\boldsymbol{g}_t)$ representing the volume density of crystals with orientation $\boldsymbol{g}_t$ at time t follows the conservation equation (2) as:

$$\int \mathcal{A}(\boldsymbol{g}_o, t=0)d\boldsymbol{g}_o = \int \mathcal{A}(\boldsymbol{g}_t)d\boldsymbol{g}_t = 1 \tag{4}$$

where $d\boldsymbol{g}_o$ represents the volume element in the undeformed (initial) ODF mesh which becomes volume element $d\boldsymbol{g}_t$ at time t. A Jacobian $J(\boldsymbol{g}_o,t) = \det(\boldsymbol{G})$ gives the ratio of elemental volumes, where $\boldsymbol{G}$ is the reorientation gradient given as $\boldsymbol{G}(\boldsymbol{g}_o,t) = \frac{\partial \boldsymbol{g}_t}{\partial \boldsymbol{g}_o}$. Using the Jacobian, a map of the current mesh (at time t) to the reference mesh (at $t = 0$) can be made (assuming the map is invertible):

$$\int (\mathcal{A}(\boldsymbol{g}_o, t=0) - \hat{\mathcal{A}}(\boldsymbol{g}_o,t)J(\boldsymbol{g}_o,t))d\boldsymbol{g}_o = 0 \tag{5}$$

The quantity written as $\hat{\mathcal{A}}(\boldsymbol{g}_o,t)$ is the volume density $\mathcal{A}(\boldsymbol{g}_t)$ plotted over the corresponding orientation $(\boldsymbol{g}_o)$ in the initial mesh. Thus, $\hat{\mathcal{A}}(\boldsymbol{g}_o,t)$ gives the Lagrangian representation of the current ODF in the initial mesh. If the integrand is continuous, a localized relationship of the following form can be used to update the ODF at any time t:

$$\hat{\mathcal{A}}(\boldsymbol{g}_o,t) = \frac{\mathcal{A}(\boldsymbol{g}_o, t=0)}{J(\boldsymbol{g}_o,t)} \tag{6}$$

Fig. 2 gives an idea of how the approach works for a one-dimensional fundamental region that is represented using two-noded finite elements with linear interpolation. Here, the Jacobian is simply the ratio of element lengths, i.e. current length divided by the initial length. If the element length decreases over time, the probability density has to increase based on Eq. (6) to maintain normalization of the ODF. A similar approach is used to update the probability density $\mathcal{F}$ in the mesh $M_{g'|gr}$ as follows:

$$\hat{\mathcal{F}}(\boldsymbol{g}_t'|(\boldsymbol{g}_t,\boldsymbol{r}_o,t)) = \frac{\mathcal{F}(\boldsymbol{g}_o', t=0|(\boldsymbol{g}_o,\boldsymbol{r}_o))}{J(\boldsymbol{g}_o',t)} \tag{7}$$

2.2. Interaction law

The microstructure is discretized into pixels (Fig. 3(a)) center pixel $\boldsymbol{x}$ is assumed to only interact with the four

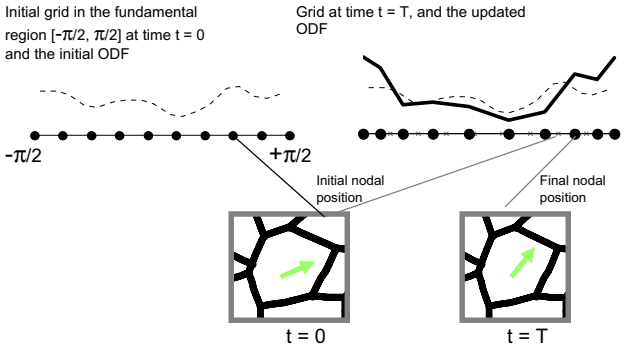

Fig. 2. Probability update scheme in FE space: During deformation, the nodal points ($\boldsymbol{g}$) of the FE mesh are moved to reflect reorientation ($\Delta\boldsymbol{g}$) of crystals. The new ODF is obtained using Eq. (6) that ensures that the normalization constraint (Eq. (4)) is met in the reoriented mesh.

neighbor pixels $\boldsymbol{x}_i'$ ($i = 1,\ldots,4$, with each particle occupying area ΔA_i) along a bond defined by the vector $\langle \boldsymbol{x}_i' - \boldsymbol{x}\rangle$ as shown in Fig. 3(b).

The equation of balance of linear momentum at time t for the center pixel $\boldsymbol{x}$ (assuming quasi-static loading and no body forces) is given by [24]:

$$\boldsymbol{L}(\boldsymbol{x}) = \sum_{i=1}^{4}\left\{\boldsymbol{T}[\boldsymbol{x}]\langle \boldsymbol{x}_i' - \boldsymbol{x}\rangle - \boldsymbol{T}\left[\boldsymbol{x}_i'\right]\langle \boldsymbol{x} - \boldsymbol{x}_i'\rangle\right\}\Delta A_i = 0 \tag{8}$$

where the term $\boldsymbol{T}[\boldsymbol{x}]\langle \boldsymbol{x}' - \boldsymbol{x}\rangle$ is the force state on pixel $\boldsymbol{x}$ operating on the bond $\langle \boldsymbol{x}' - \boldsymbol{x}\rangle$. A typical configuration of pixels of equal area is shown in Fig. 3(b). For this configuration, force state $\boldsymbol{T}$ can be modeled as,

$$\begin{aligned}\boldsymbol{T}[\boldsymbol{x}]\langle \boldsymbol{x}_i' - \boldsymbol{x}\rangle &= \boldsymbol{P}^x(\boldsymbol{x}_i' - \boldsymbol{x})\\ \boldsymbol{T}\left[\boldsymbol{x}_i'\right]\langle \boldsymbol{x} - \boldsymbol{x}_i'\rangle &= \boldsymbol{P}^i(\boldsymbol{x} - \boldsymbol{x}_i')\end{aligned} \tag{9}$$

where $\boldsymbol{P}$ denotes the first Piola–Kirchhoff stress with the superscripts denoting the particle number (x is the center pixel and $i = 1,2,3,4$ denoting the four neighbor pixels as shown in Fig. 3(b). By plugging in the coordinates and the stresses of the five pixels in Eq. (8), the following equilibrium equations are obtained in terms of the stress components (written as subscripts):

$$\begin{aligned}P_{11}^3 + P_{12}^1 - P_{11}^2 - P_{12}^4 &= 0\\ P_{21}^3 + P_{22}^1 - P_{21}^2 - P_{22}^4 &= 0\end{aligned} \tag{10}$$

In the statistical model, the stress $\boldsymbol{P}^k$ of pixel k is replaced by a homogenized stress $\langle \boldsymbol{P}^k\rangle$ found by averaging the PK stress of each orientation over the initial NNOCF $\mathcal{F}^k(\boldsymbol{g}_o', t=0|(\boldsymbol{g}_o,\boldsymbol{r}_o))$ at pixel k, ie,

$$\langle \boldsymbol{P}^k\rangle = \int \hat{\boldsymbol{P}}\mathcal{F}^k d\boldsymbol{g}_o' = \sum_{l=1}^{N}\hat{\boldsymbol{P}}^l\mathcal{F}^{kl}\Delta V^l \tag{11}$$

The quantity written as $\hat{\boldsymbol{P}}$ is the stress $\boldsymbol{P}(\boldsymbol{g}_t')$ plotted over the corresponding orientation $(\boldsymbol{g}_o')$ in the initial NNOCF mesh (ie. the Lagrangian representation). Superscript l denotes the node ($l = 1,\ldots,N$, N is the number of independent nodes) in the NNOCF mesh at pixel k. ΔV^l is the volume assigned to node l in the orientation space.

Equilibrium is enforced by minimizing the equilibrium equations with respect to the deformation gradient of each orientation. At each time step, an initial guess for the

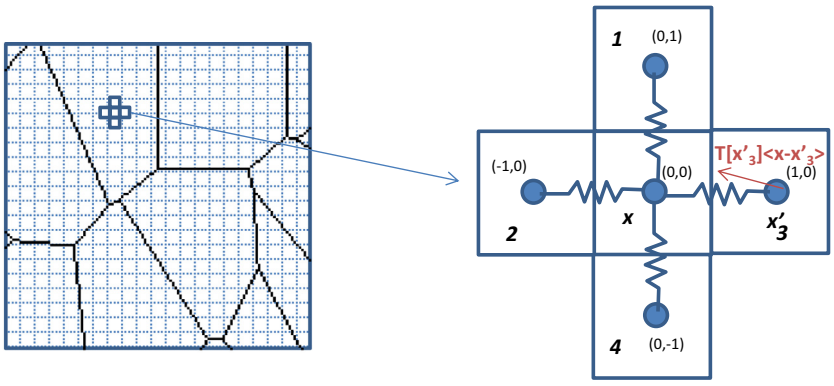

Fig. 3. (a) Microstructure is discretized into pixels and interaction of pixel x (center pixel) with four nearest neighbors is modeled. (b) The coordinates of a pixel configuration (in pixel units). The force exerted by pixel 3 on the x is denoted by $\boldsymbol{T}[\boldsymbol{x}'_3]\langle \boldsymbol{x}-\boldsymbol{x}'_3\rangle$.

deformation gradient of orientation l, $\boldsymbol{F}^l_{taylor}$, is computed based on a Taylor approximation for the velocity gradient ($\boldsymbol{L}^l = \boldsymbol{L}^{macro}$). A finite difference formula is used, ie.,

$$\boldsymbol{F}^l_{taylor} = (\boldsymbol{I} - \boldsymbol{L}^{macro}\Delta t)\boldsymbol{F}^l_{prev} \tag{12}$$

where $\boldsymbol{F}^l_{prev}$ is the (corrected) deformation gradient known from the previous time step. For simplifying the notation, the deformation gradient tensor (in 2D) for the orientation at node l is denoted in a vector form such that: $\check{F}^l_1 = F^l_{11}$, $\check{F}^l_2 = F^l_{12}$, $\check{F}^l_3 = F^l_{21}$, $\check{F}^l_4 = F^l_{22}$. The variation of stress tensor with respect to the deformation gradient is of the form:

$$\delta\langle P^k_{ij}\rangle = \sum_{l=1}^{N}\mathcal{F}^{kl}\Delta V^l\left(\sum_{q=1}^{4}\frac{\partial \hat{P}^l_{ij}}{\partial \check{F}^l_q}\delta\check{F}^l_q\right) \tag{13}$$

Here, the PK stress $\hat{\boldsymbol{P}}$ and the tangent modulus $\frac{\partial \hat{\boldsymbol{P}}}{\partial \boldsymbol{F}}$ are evaluated using the crystal plasticity constitutive model at a deformation gradient of $\boldsymbol{F}^l_{taylor}$. A Newton Raphson scheme of the following form is then set-up to compute the corrections $\delta\check{\boldsymbol{F}}^l$ to the Taylor model:

$$\begin{aligned}
&\delta\langle P^3_{11}\rangle + \delta\langle P^1_{12}\rangle - \delta\langle P^2_{11}\rangle - \delta\langle P^4_{12}\rangle \\
&\quad = -(\langle P^3_{11}\rangle + \langle P^1_{12}\rangle - \langle P^2_{11}\rangle - \langle P^4_{12}\rangle) \\
&\delta\langle P^3_{21}\rangle + \delta\langle P^1_{22}\rangle - \delta\langle P^2_{21}\rangle - \delta\langle P^4_{22}\rangle \\
&\quad = -(\langle P^3_{21}\rangle + \langle P^1_{22}\rangle - \langle P^2_{21}\rangle - \langle P^4_{22}\rangle)
\end{aligned} \tag{14}$$

An additional set of equations is augmented to the above system in order to ensure that the average deformation gradient remains the same as the macroscopic deformation gradient applied to the microstructure [22], i.e., $\int \boldsymbol{F}(\boldsymbol{g}_o,t)\mathcal{A}(\boldsymbol{g}_o,t=0)d\boldsymbol{g}_o = \boldsymbol{F}^{macro}$. Since the initial guess based on the Taylor assumption already satisfies this, it is enough to ensure that the increment in deformation gradient averages to zero over all orientations. In other words, $\int \delta\boldsymbol{F}\mathcal{A}d\boldsymbol{g}_o = 0$, or in the discretized form:

$$\sum_{l=1}^{N}\delta\check{F}^l_q A^l \Delta V^l = 0, \quad q = 1,\ldots,4 \tag{15}$$

The above equation (Eq. (15)) is augmented to Eq. (14) and the resulting set of equations are arranged in a matrix–vector form (using Eq. (13)) as: $\mathcal{J}\delta\check{\boldsymbol{F}} = \boldsymbol{R}$ where $\delta\check{\boldsymbol{F}} = [\delta\check{F}^1_1, \delta\check{F}^1_2, \delta\check{F}^1_3, \delta\check{F}^1_4, \delta\check{F}^2_1, \delta\check{F}^2_2, \ldots, \delta\check{F}^N_3, \delta\check{F}^N_4]^T$. Since this is an underdetermined system, the solution is obtained using a pseudo-inverse operation which gives the correction with the minimum Euclidean norm $\|\delta\check{\boldsymbol{F}}\|_2$. The equation is solved only once and a step size (λ) is used to correct the deformation gradient of orientation l as: $\check{\boldsymbol{F}}^l_{corrected} = \check{\boldsymbol{F}}^l_{taylor} + \lambda\delta\check{\boldsymbol{F}}^l$.

2.3. Constitutive modeling

A single-crystal constitutive model [24] is employed to model the plastic flow that takes place through slip on prescribed slip systems. For a material with $\alpha = 1,\ldots,N$ slip systems defined by ortho-normal vector pairs $(\boldsymbol{m}^\alpha_0, \boldsymbol{n}^\alpha_0)$ denoting the slip direction and slip plane normal respectively at time $t = 0$, the constitutive equations relate the following basic fields (all quantities expressed in crystal lattice coordinate frame): the deformation gradient $\boldsymbol{F}$ defined with respect to the initial undeformed crystal which can be decomposed into elastic and plastic parts as $\boldsymbol{F} = \boldsymbol{F}^e\,\boldsymbol{F}^p$ (with $\det(\boldsymbol{F}^p) = 1$), the Cauchy stress $\boldsymbol{\sigma}$ and the slip resistances $s^\alpha > 0$. In the constitutive equations to be defined below, the Green elastic strain measure $\bar{\boldsymbol{E}}^e = \frac{1}{2}(\boldsymbol{F}^{eT}\boldsymbol{F}^e - \boldsymbol{I})$ defined on the relaxed configuration (plastically deformed, unstressed configuration $\bar{\mathcal{B}}$) is utilized. The conjugate stress measure is then defined as $\bar{\boldsymbol{T}} = \det\boldsymbol{F}^e(\boldsymbol{F}^e)^{-1}\boldsymbol{\sigma}(\boldsymbol{F}^e)^{-T}$.

The constitutive relation, for stress, is given by $\bar{\boldsymbol{T}} = \mathbb{C}[\bar{\boldsymbol{E}}^e]$ where $\mathbb{C}$ is the fourth-order anisotropic elasticity tensor. It is assumed that deformation takes place through dislocation glide and the evolution of the plastic velocity gradient is given by:

$$\boldsymbol{L}^p = \dot{\boldsymbol{F}}^p(\boldsymbol{F}^p)^{-1} = \sum_\alpha \dot{\gamma}^\alpha \boldsymbol{S}^\alpha_0 sign(\tau^\alpha) \tag{16}$$

where $\boldsymbol{S}^\alpha_0 = \boldsymbol{m}^\alpha_0 \otimes \boldsymbol{n}^\alpha_0$ is the Schmid tensor and $\dot{\gamma}^\alpha$ is the plastic shearing rate on the αth slip system. The resolved stress on the αth slip system is given by $\tau^\alpha = \bar{\boldsymbol{T}}\cdot\boldsymbol{S}^\alpha_0$.

A rate independent algorithm is employed to solve the single crystal model. The resolved shear stress τ^α is taken to attain a critical value s^α (the slip system resistance) on the systems where slip occurs. These active systems have a plastic shearing rate $\dot{\gamma}^\alpha > 0$. There is no plastic shearing rate ($\dot{\gamma}^\alpha = 0$) on inactive slip systems where the resolved shear stress does not exceed s^α. The evolution of slip system resistance given by the following expression:

Table 1. Algorithm for NNOCF evolution.

(1) Initialize meshes M_g and $M_{g'|rg}$ and load probabilities $\mathcal{A}(g)$ and $\mathcal{F}(g'|(r,g))$ computed from the sampling algorithm. Use $\boldsymbol{F}^l_{prev} = \boldsymbol{I}$ for all ODF nodes at $t = 0$.
(2) Apply time increment Δt.
(3) At current time step:
  (3.1) Compute guess (Taylor) deformation gradient $\check{\boldsymbol{F}}^l_{taylor}$ from Eq. (12).
  (3.2) Call constitutive model at each node (in mesh M_g) to compute the stress tensor and tangent moduli (without updating the state variables).
  (3.3) Set up the system of equations in Eqs. (15) and (14) and solve for the correction to deformation gradient $\delta\check{\boldsymbol{F}}^l$
  (3.4) Correct the deformation gradient of orientation l as: $\check{\boldsymbol{F}}^l_{corrected} = \check{\boldsymbol{F}}^l_{taylor} + \lambda\delta\check{\boldsymbol{F}}^l$
(4) Update Probabilities:
  (4.1) Call constitutive model at each node (in mesh M_g) to compute reorientation velocities at nodes in the fundamental region (use corrected deformation gradient found in step (3.4), update the state variables).
  (4.2) Update the nodal positions in the M_g and $M_{g'|rg}$ meshes using the computed reorientation velocity
  (4.3) Postprocess: Find new ODF and NNOCFs using Eqs. (6) and (7) and compute averaged stresses and strains
(5) Go to step (2) if time $t < t_{final}$

$$\dot{s}^\alpha(t) = \sum_\beta h^{\alpha\beta}\dot{\gamma}^\beta(t), \quad \text{with } s^\alpha(0) = \tau^\alpha_0 \tag{17}$$

Here, $h^{\alpha\beta}$ is the slip system hardening term, $\dot{\gamma}^\beta$ is the plastic shearing rate on the βth slip system, and τ^α_0 is the initial slip system resistance on the αth slip system. The algorithm for computing the Piola–Kirchhoff-I stress and the tangent modulus using this model is described in detail in [24].

2.4. Overall algorithm

The algorithm for the NNOCF update is given in Table 1. In the algorithm, we first compute the stress response of each orientation $\boldsymbol{g}$ using a guess deformation gradient. Subsequently, the corrected deformation gradient is computed using the nearest neighbor interaction model. The corrected deformation gradient is used to update the ODF and NNOCF. A total lagrangian approach is used where the fundamental region mesh for $\boldsymbol{g}$ and $\boldsymbol{g}'$ remain unchanged and the reorientations are only stored at the nodal points. If the reorientations are used to move the nodal locations, new orientation spaces are obtained, which are also valid fundamental regions [11]. The total Lagrangian approach used in this work is adequate for moderate strains. At larger strains, the nodal points may begin to overlap and interpenetrate. To address such situations, remeshing techniques and updated lagrangian methods need to be developed in the future.

3. Numerical examples

The improvement in prediction of texture and stresses achieved by the NNOCF approach over ODF-based methods has been quantified through simple deformation analysis of a planar polycrystalline microstructure. Orientations of planar crystals are characterized by the two dimensional rotation $\boldsymbol{R}$ relating the crystal lattice frame to the reference sample frame. A parametrization of the associated rotation group is,

$$\boldsymbol{R} = \boldsymbol{I}cos(\boldsymbol{r}) - \boldsymbol{E}sin(\boldsymbol{r}) \tag{18}$$

where $\boldsymbol{r}$ is the angle between the crystal and sample axes, $\boldsymbol{E}$ is the two dimensional alternator ($E_{11} = E_{22} = 0$, $E_{12} = -E_{21} = 1$), and $\boldsymbol{I}$ is the identity tensor. Under the symmetry, crystal orientations can be described uniquely by parameters drawn from a simply connected fundamental region $[a, a+\pi)$. Out of convenience, we will restrict the choice of fundamental regions to the interval closest to the origin $(-\pi/2, \pi/2)$. Due to symmetry, the orientation $\pi/2$ is exactly the same as orientation $-\pi/2$. This constraint on the ODF and NNOCF is enforced in practise by using periodic boundary conditions in the finite element mesh. The crystal reorientation velocity follows by taking a derivative of relation Eq. (18):

$$\boldsymbol{v} = \frac{1}{2}E \cdot \boldsymbol{\Omega} \tag{19}$$

where $\boldsymbol{\Omega}$ is the spin tensor defined as $\boldsymbol{\Omega} = \dot{\boldsymbol{R}}^e\boldsymbol{R}^{eT}$. Here, $\boldsymbol{R}^e$ is evaluated through the polar decomposition of the elastic deformation gradient $\boldsymbol{F}^e = \boldsymbol{R}^e\boldsymbol{U}^e$ in the constitutive model.

Nine different orientations from within the interval $(-\pi/2, \pi/2)$ were distributed among the grains. The values in the elastic stiffness matrix are taken as $\mathbb{C}_{11} = 2$ GPa and $\mathbb{C}_{12} = \mathbb{C}_{44} = 1$ GPa. A specific crystal geometry with two slip systems at orientation $-\pi/6$ and $+\pi/6$ was considered. The particular hardening law in Eq. (17) is modeled as $h^{\alpha\beta} = h_o(q + (1-q)\delta^{\alpha\beta})$ with $h_o = 20$ MPa as the hardening constant, $q = 1.4$ as the latent hardening parameter and $\tau_0 = 20$ MPa as the initial slip system resistance value (taken to be identical for both slip systems). A step size of $\lambda = 0.02$ was chosen. The imposed macroscopic velocity gradients $\boldsymbol{L}$ in the examples are:

$$\boldsymbol{L} = \eta\begin{bmatrix}1 & 0\\ 0 & -1\end{bmatrix} \quad \text{(Y-axis compression)} \tag{20}$$

and

$$\boldsymbol{L} = \eta\begin{bmatrix}2 & 0\\ 0 & 0\end{bmatrix} \quad \text{(X-axis shear)} \tag{21}$$

Here η is a constant strain rate taken to be 0.016/s.

To test the proposed formulation, a representative volume element (RVE) made using a Voronoi tessellation was chosen. Fig. 4(a) shows the initial microstructure as well as the initial ODF and NNOCF sampled from the RVE using methods described in [19]. The initial ODF and NNOCF are plotted on a finite element grid with nine line elements in the fundamental region $(-\pi/2, \pi/2)$ of a planar microstructure (with element length $\Delta V = \pi/9$) and are shown in Fig. 4(b). In this visualization, the ODF $\mathcal{A}(\boldsymbol{g})$ is shown at the center. The NNOCFs along each of the four directions from $\boldsymbol{g}$ are shown as colored matrices. In this matrix, the column i represents the NNOCF (ie.

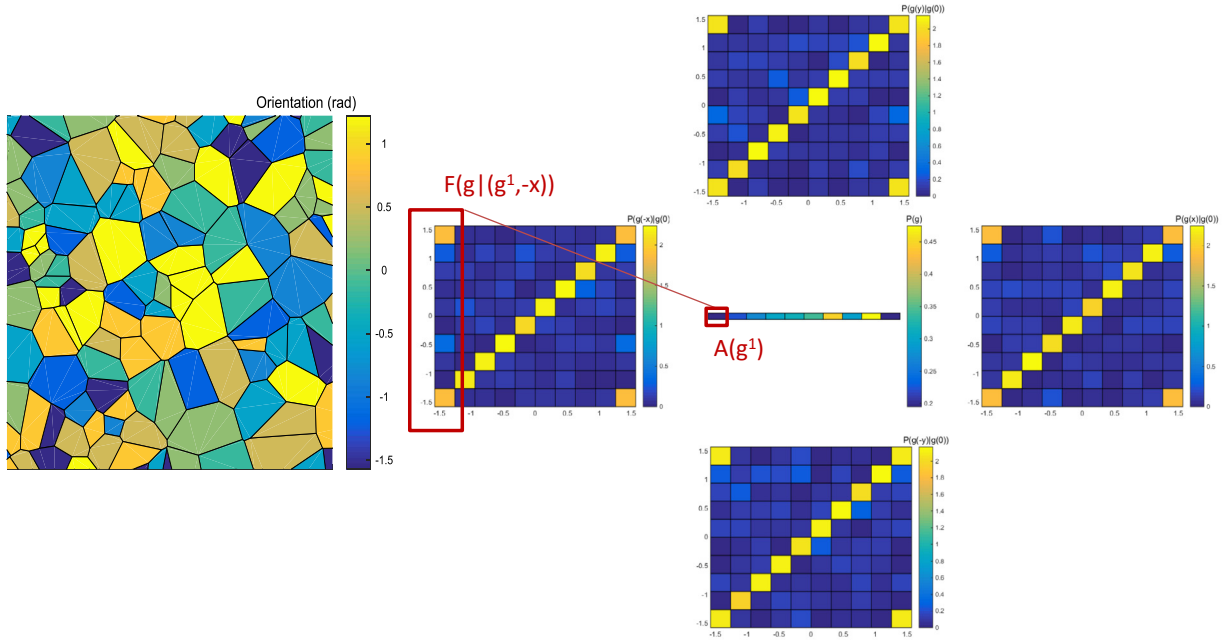

Fig. 4. (a) Microstructure consisting of about 100 grains colored by the grain orientation. (b) The statistical descriptor: ODF is plotted in the center. The NNOCF for the four neighbor pixels of each orientation are also plotted. The red boxes show the orientation distribution (A) of g^1 and the distribution (F) for the left neighbor pixel of g^1. (For interpretation of the references to color in this figure legend, the reader is referred to the web version of this article.)

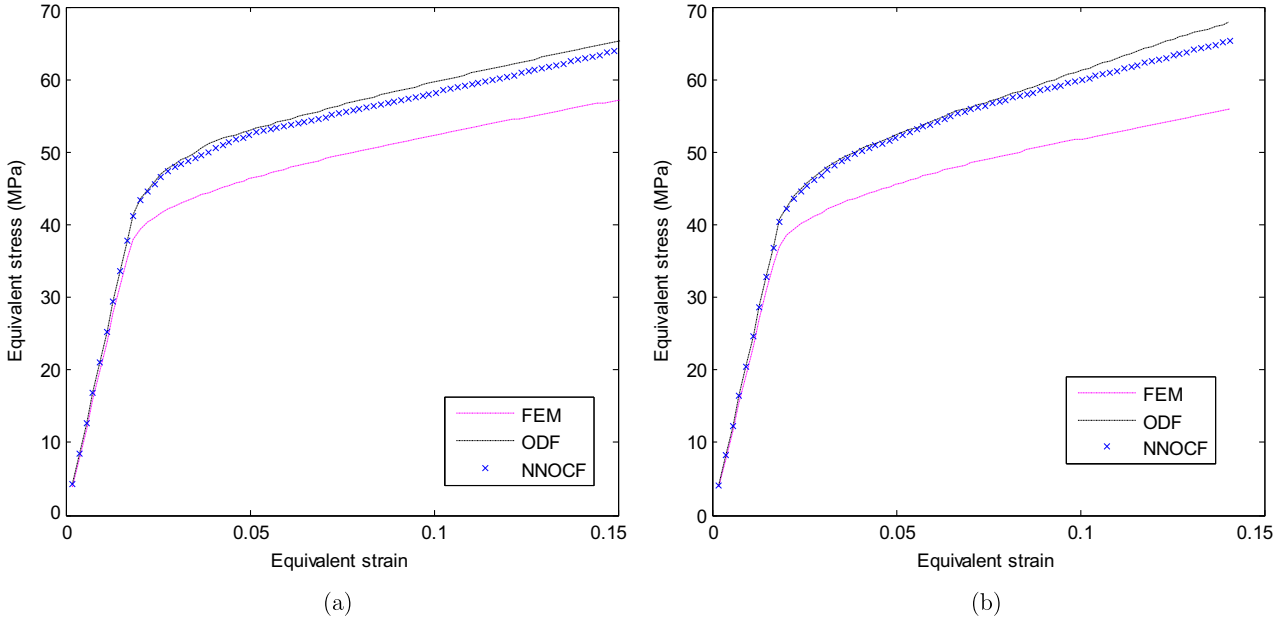

Fig. 5. Comparison of equivalent stress–strain response predicted by the ODF, NNOCF and the CPFE model for (a) Y-axis compression test (b) X-axis shear test.

$\mathcal{F}(\boldsymbol{g}'|(\boldsymbol{g}^i,\boldsymbol{r}))$ corresponding to i^{th} node of the ODF (ie. orientation $\boldsymbol{g}^i$). The diagonals of the matrix have significantly higher probability since it is much more likely for a pixel (eg. within a grain) to be surrounded by like orientations. The smaller probabilities seen in the off-diagonals account for the pixels at the grain boundaries of each grain. Within the diagonal values, higher color intensities give a measure of relative grain size in that direction. For example, grains with orientation of -1.5 (darkest blue grains in Fig. 4(a)) are longer in the y-direction on average; which is reflected in higher NNOCF intensities in the vertical direction compared to the horizontal directions (corner values of the matrix). The corner points are identical due to crystallographic symmetry.

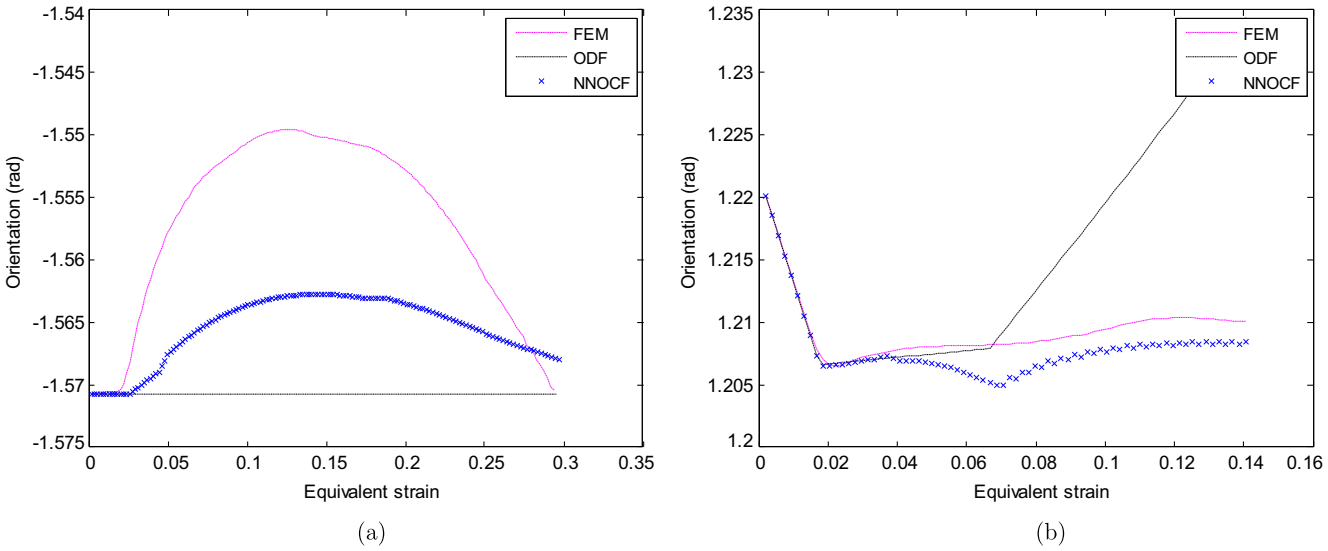

Fig. 6. Comparison of orientation change predicted by the ODF, NNOCF and the CPFE model for (a) $-\pi/2$ orientation during Y-axis compression. The ODF (Taylor) model predicts no change in orientation. However, orientation changes to maintain equilibrium across grain boundaries. This is captured by both NNOCF and CPFE models. (b) $7\pi/18$ orientation during X-axis shear. Here, a sharp increase in orientation is predicted at a strain of 0.075 by the Taylor model. Both CPFE and NNOCF models predict a more gradual change due to interactions with neighbor grains.

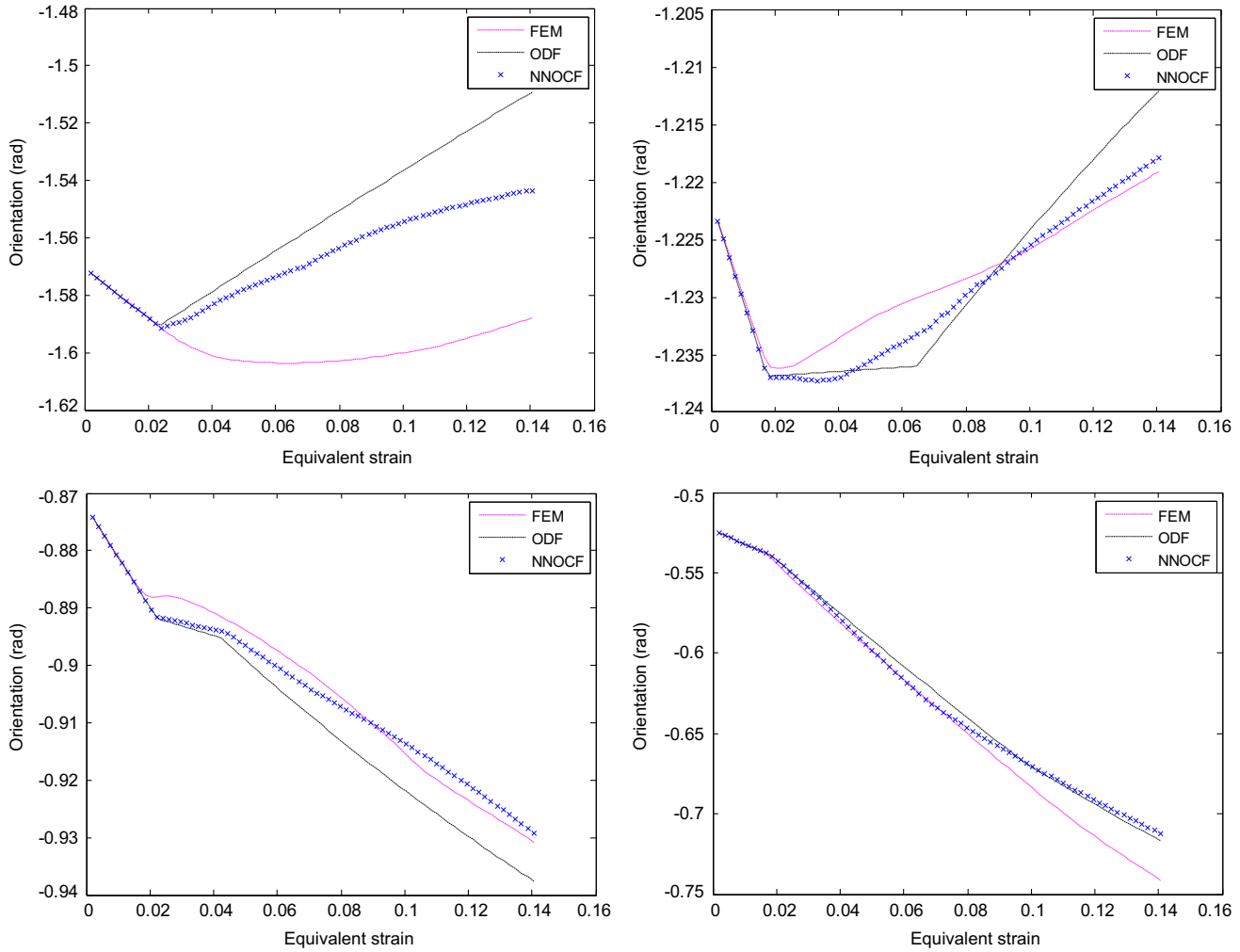

Fig. 7. Comparison of orientation change predicted by the ODF, NNOCF and the CPFE model for nodes 1 to 4 in the ODF mesh during x-axis shear.

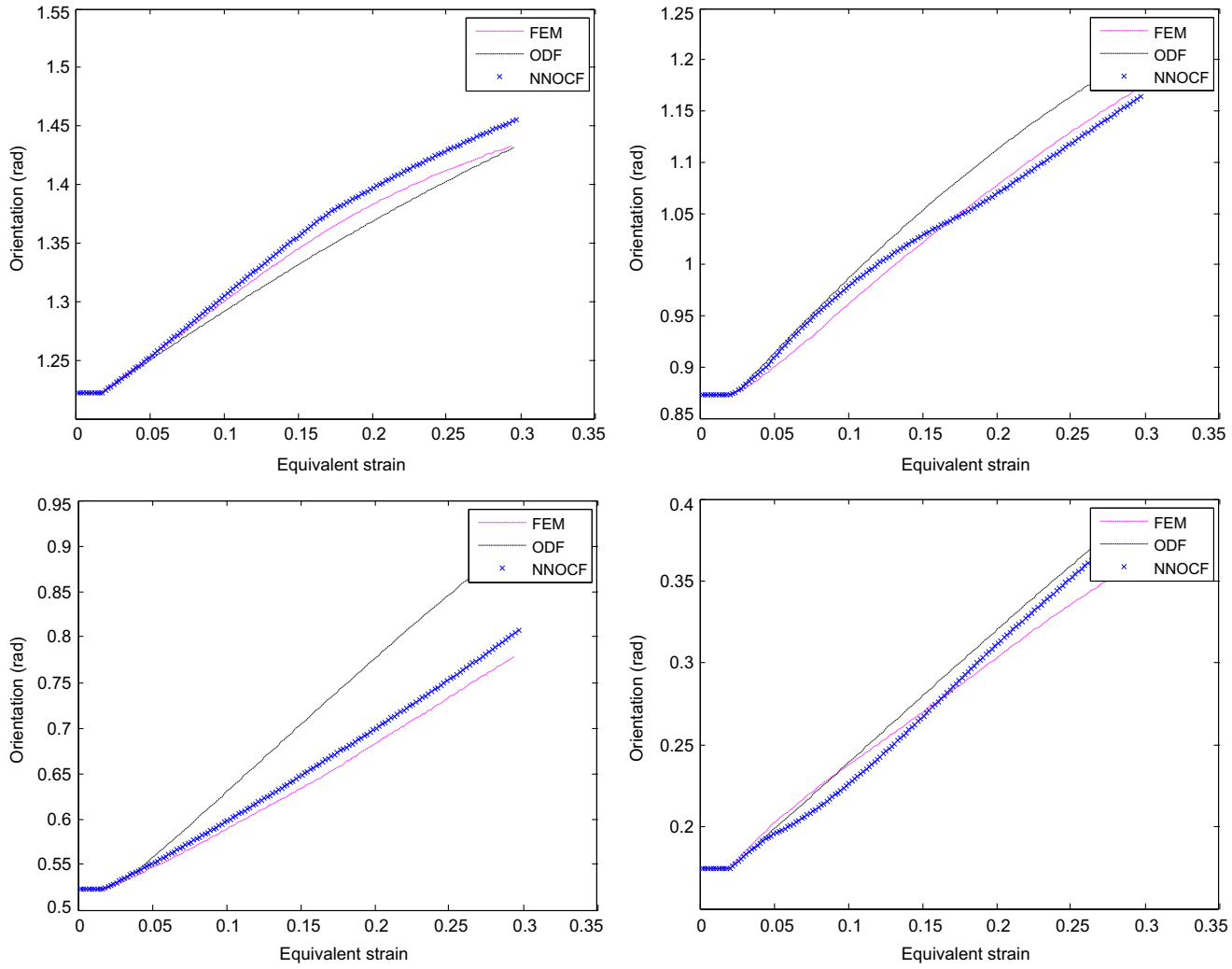

Fig. 8. Comparison of orientation change predicted by the ODF, NNOCF and the CPFE model for nodes 6 to 9 in the ODF mesh during y-axis compression.

In order to test the approach, the NNOCF simulation results are compared against the more accurate crystal plasticity finite element (CPFE) method. CPFE explicitly models the microstructure and enforces both compatibility and equilibrium across grain boundaries. Here, CPFE is considered the ground truth model. The results are also compared against an ODF model that employs the Taylor assumption. The equivalent stress–strain response for all three models are compared in Fig. 5 for compression as well as shear test. The ODF model does not satisfy equilibrium and leads to a stiff upper bound response. Although the NNOCF model gives little to no improvement from the ODF result at small strains, modest improvements are seen at larger strains with the NNOCF result trending towards the CPFE result.

The strength of the NNOCF model, however, is its ability to predict texture components that are missed entirely by the ODF model. For example, during y-axis compression, $-\pi/2$ orientation is favorably aligned with the compression axis and the ODF model indeed predicts no change in this orientation with deformation (as shown in Fig. 6(a)). On the other hand, CPFE predicts that this orientation should change gradually because the orientation is unfavorably aligned to the inhomogeneous local deformation state of its neighborhood grains. A similar trend is indeed predicted by the NNOCF model. Another example for $7\pi/18$ orientation during X-axis shear is shown in Fig. 6(b). Here, a sharp increase in orientation is predicted at a strain of 0.075 by the Taylor model, while both CPFE and NNOCF models predict a more gradual change due to interactions with neighbor grains.

When making the comparison of ODF/NNOCF models with the CPFE model in Fig. 6(a), note that each grain with $-\pi/2$ orientation in the CPFE model behaves differently depending on its neighborhood. The ODF or NNOCF models, in contrast, capture an average change for each orientation. Thus, to reliably compare the probabilistic models with the CPFE model, one needs to average the orientation change of all grains in the CPFE model with the same initial orientation. The prediction of average changes in grain orientation as seen in the evolution of several other orientations is shown in Figs. 7 and 8. Fig. 7 compares the orientation change predicted by the ODF, NNOCF and the CPFE model for nodes 1 to 4 in the ODF mesh during x-axis shear. Fig. 8 compares the orientation change predicted by the ODF, NNOCF and the CPFE model for nodes 6 to 9 in the ODF mesh during y-axis compression. As seen from these plots, the use of

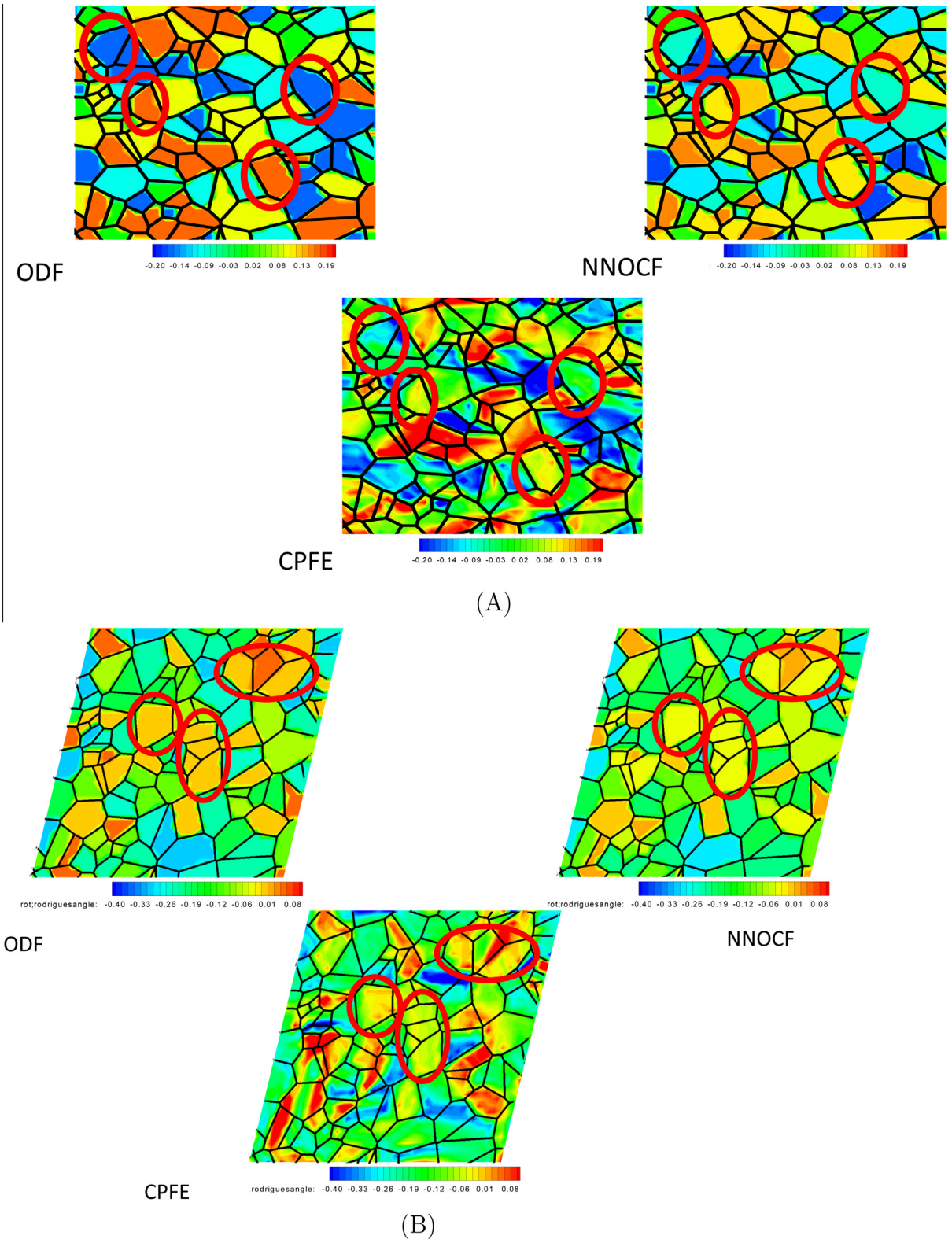

Fig. 9. Comparison of orientation change predicted by the ODF, NNOCF and the CPFE model at 7.5 s during *y*-axis compression (A) and *x*-axis shear (B). Regions of the microstructure where the use of NNOCF information leads to significant changes in reorientation prediction are highlighted.

neighborhood information (via the NNOCF) leads to significantly better prediction of texturing in comparison to the ODF model.

The differences between the CPFE and NNOCF models in predicted textures is primarily due to the use of averaged neighborhood information in the NNOCF model. In other

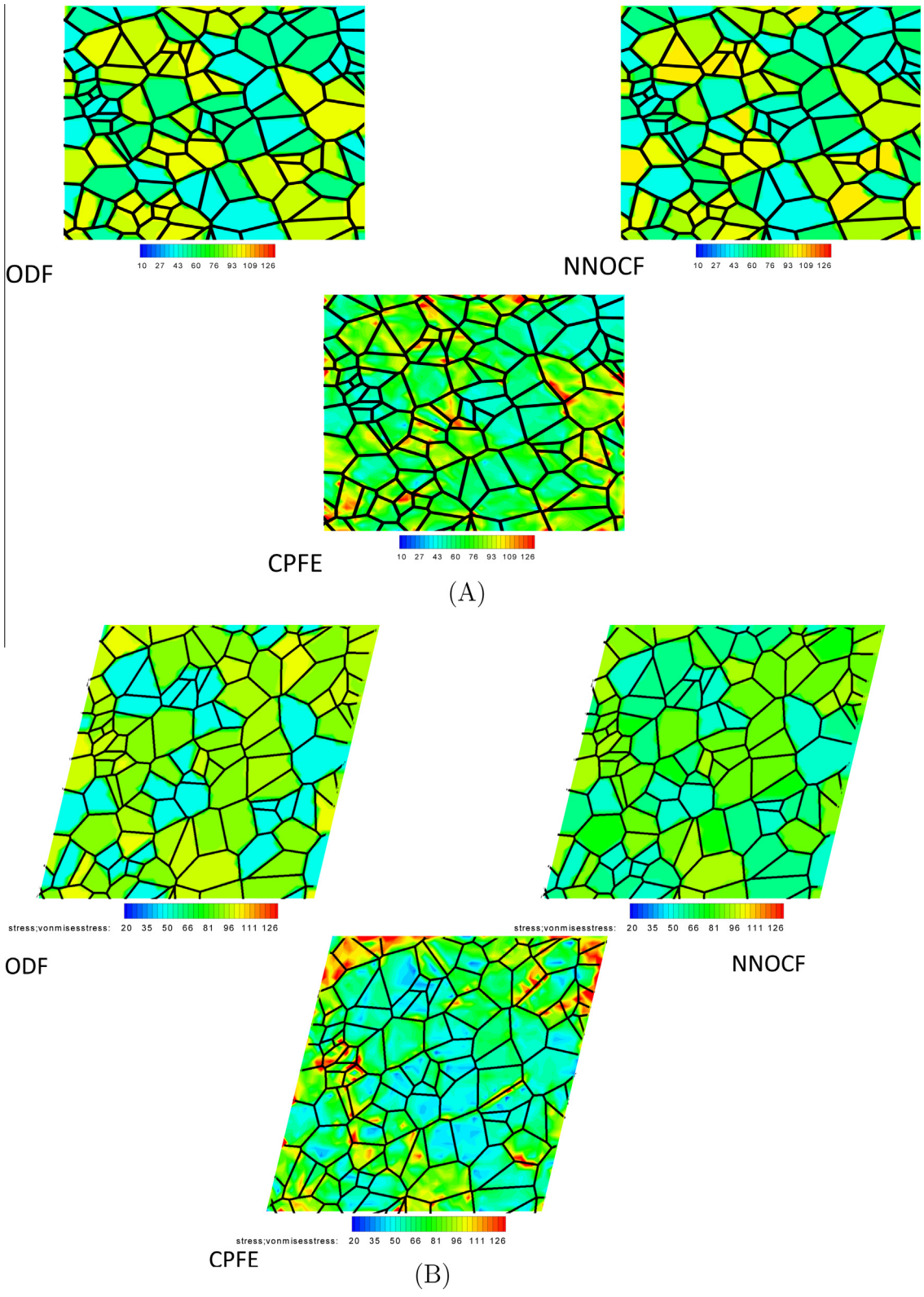

Fig. 10. Comparison of equivalent stress at 7.5 s during y-axis compression (A) and x-axis shear (B).

words, NNOCF model overlooks the differences in local neighborhood for grains that have the same orientation but are located at different positions in the microstructure. Alternatively, the NNOCF results shown here can be seen as an ensemble average obtained for all microstructures with the given initial two-point descriptor. In contrast, the CPFE solution shown here provides a single sample from this large ensemble of microstructures. In order to visually interpret the results of the NNOCF and ODF models against the CPFE model, we have plotted the microstructural fields in Figs. 9 and 10. Since the ODF and NNOCF models work in the orientation space and

do not compute the fields over a microstructure (unlike the CPFE model), we have superposed the orientation changes and stresses for each grain over a pixel grid of the microstructure. Comparison of orientation change predicted by the ODF, NNOCF and the CPFE model at 7.5 s during y-axis compression and x-axis shear are shown in Fig. 9(A) and (B), respectively. Regions of the microstructure where the use of NNOCF information leads to significant changes in reorientation prediction as compared to the ODF model are circled. The reorientation in these regions as predicted by the NNOCF model favorably compares to those predicted by the CPFE model. CPFE model predicts heterogeneous misorientation development even within each grain, as dictated by global equilibrium. Although the NNOCF model cannot model the intragranular heterogeneity, the average misorientation within each grain is well predicted, as seen previously in Figs. 7 and 8.

The equivalent stress response for these models at 7.5 s during y-axis compression and x-axis shear are compared in Figs. 8 and 10(B), respectively. Although, in an average sense (as seen in Fig. 5), the NNOCF results trend towards the CPFE model, the stresses predicted by the CPFE model are in stark contrast to those predicted by the ODF/NNOCF models. There are intense regions of stresses (banding) surrounded by regions of relatively lower stresses. Such stress concentrations cannot be modeled using the present approach. However, the regions of stress concentrations are seen to coincide mostly with the grains predicted to have higher stresses in the NNOCF model.

While the data presented so far are based on one microstructure realization, we looked at the model performance over 30 different microstructures to check if the results could be generalized. Each microstructure was constructed using different voronoi tessellations and the grain orientations were randomly assigned. The microstructures were subjected to x-axis shear deformation for 5 s. The l_2 norm of the difference in reorientation and equivalent stress predictions (as a function of time) of the NNOCF and ODF models with respect to the CPFE model was compared. The improvement of the NNOCF model over the ODF model is shown in Fig. 11(a). The bars in Fig. 11(a) indicate the average of 30 cases, and the improvements in prediction of each individual microstructure are shown as a scatter plot. The plot shows that the use of NNOCF information reduces the error in prediction of stresses and orientations by 25% on average when compared to the Taylor model. The individual improvements range from 13% to as much as 48% in prediction of reorientation and between 11% and 34% in the prediction of equivalent stresses.

More importantly, the decrease in error is achieved with a significantly less computational cost compared to the CPFE model. Fig. 11(b) shows comparison of simulation speed of CPFE model with respect to NNOCF model and ODF model. NNOCF model is 45 times faster than CPFE although it is about 4 times slower than the ODF model.

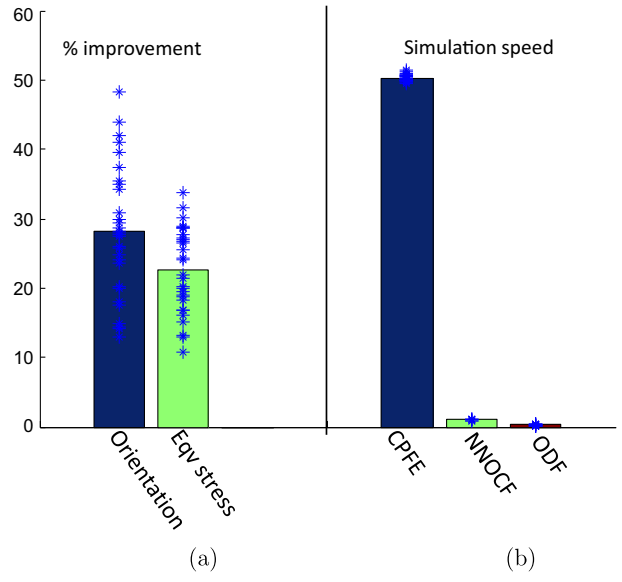

Fig. 11. (a) NNOCF model reduces the error in prediction of stresses and orientations on an average of about 25% when compared to the Taylor model. The bars indicate the average of 30 cases, and the improvements in prediction of each individual microstructure are shown as a scatter. The individual improvements range from 13% to as much as 48% in prediction of reorientation. (b) Comparison of simulation speed of CPFE model with respect to NNOCF model and ODF model. NNOCF model is 45 times faster than CPFE although it is about 4 times slower than the ODF model.

4. Conclusion

In this paper, a probabilistic model based on nearest neighbor conditional orientation correlation function (NNOCF) was used for modeling microstructure evolution during deformation. The NNOCF approach is an attempted move towards a new regime of computation where instead of microstructures, probabilistic descriptors are represented and evolved. The NNOCF describes the probability density of occurrence of a crystal orientation $\boldsymbol{g}'$ at one pixel distance $\boldsymbol{r}$ from a given orientation $\boldsymbol{g}$. The neighborhood information obtained from this function is used to correct a Taylor-based formulation of crystal plasticity. The interaction between neighboring orientations was modeled using a novel finite differencing scheme.

To show the relevance of this work to the material community, we have performed comparison of our new approach to well-established ODF and crystal plasticity finite element approaches. Testable predictions are made in cases where the NNOCF model captures texture components that are otherwise missed entirely by the Taylor (ODF) model. Comparison with the CPFE results indicates that the NNOCF model decreases the error in prediction of texture and stresses by about 25% on average compared to the ODF (or Taylor) model. For the various cases studied, the NNOCF approach was significantly (45 times) faster than CPFE and about 4 times slower than the ODF model. The improvement in computational efficiency achieved by NNOCF models is most useful when performing multiscale design of industrial forming processes [25]. Once the initial NNOCF of the raw material (or preform) is known, the data can be used to improve accuracy in texture prediction without incurring the computational expense involved in the CPFE approach.

Acknowledgments

The work presented here was funded by Office of Naval Research (ONR) Grant N00014-12-1-0013, with Dr. William Mullins as program manager.

References

[1] J. Allison, D. Backman, L. Christodoulou, Integrated computational materials engineering: a new paradigm for the global materials profession, J. Miner. Met. Mater. Soc. 58 (2006) 25–27.

[2] S.V. Harren, R.J. Asaro, Nonuniform deformations in polycrystals and aspects of the validity of the Taylor model, J. Mech. Phys. Solids 37 (1989) 191–232.

[3] C.A. Bronkhorst, S.R. Kalidindi, L. Anand, Polycrystalline plasticity and the evolution of crystallographic texture in fcc metals, Philos. Trans. R. Soc. Lond. A 341 (1992) 443–477.

[4] A.J. Beaudoin, H. Mecking, U.F. Kocks, Development of localized orientation gradients in fcc polycrystals, Philos. Mag. A. 73 (1996) 1503–1518.

[5] G.B. Sarma, B. Radhakrishnan, P.R. Dawson, Mesoscale modeling of microstructure and texture evolution during deformation processing of metals, Adv. Eng. Mater. 4 (2002) 509–514.

[6] M.A.S. Qidwai, A.C. Lewis, A.B. Geltmacher, Using image-based computational modeling to study microstructure-yield correlations in metals, Acta Mater. 57 (2009) 4233–4247.

[7] A. Clement, Prediction of deformation texture using a physical principle of conservation, Mater. Sci. Eng. 55 (1982) 203–210.

[8] H.J. Bunge, Texture Analysis in Materials Science, first ed., Butterworths, London, 1982.

[9] B.L. Adams, J.P. Boehler, M. Guidi, E.T. Onat, Group theory and representation of microstructure and mechanical behavior of polycrystals, J. Mech. Phys. Solids 40 (1992) 723–737.

[10] S.R. Kalidindi, H.K. Duvvuru, Spectral methods for capturing crystallographic texture evolution during large plastic strains in metals, Acta Mater. 53 (2005) 3613–3623.

[11] A. Kumar, P.R. Dawson, The simulation of texture evolution using finite elements over orientation space. I. Development, Comput. Methods Appl. Mech. Eng. 130 (1996) 227–246.

[12] A. Kumar, P.R. Dawson, The simulation of texture evolution using finite elements over orientation space. II. Application to planar crystals, Comput. Methods Appl. Mech. Eng. 130 (1996) 247–261.

[13] S. Sun, V. Sundararaghavan, A probabilistic crystal plasticity model for modeling grain shape effects based on slip geometry, Acta Mater. 60 (2012) 5233–5244.

[14] G.I. Taylor, Plastic strain in metals, J. Inst. Met. 62 (1938) 307–325.

[15] U.F. Kocks, C.N. Tomé, H.R. Wenk, Texture and Anisotropy – Preferred Orientations in Polycrystals and Their Effect on Materials Properties, first ed., Cambridge University Press, Cambridge, 2000.

[16] P.B. Corson, Correlation functions for predicting properties of heterogeneous materials. II. Empirical construction of spatial correlation functions for two phase solids, J. Appl. Phys. 45 (1976) 3165–3170.

[17] H. Garmestani, S. Lin, B.L. Adams, S. Ahzi, Statistical continuum theory for large plastic deformation of polycrystalline materials, J. Mech. Phys. Solids 49 (2001) 589–607.

[18] B.L. Adams, X. Gao, S.R. Kalidindi, Finite approximations to the second-order properties closure in single phase polycrystals, Acta Mater. 53 (2005) 3563–3577.

[19] V. Sundararaghavan, A. Kumar, Probabilistic modeling of microstructure evolution using finite element representation of statistical correlation functions, Int. J. Plast. 30 (2012) 62–80.

[20] B.L. Adams, G.R. Canova, A. Molinari, A statistical formulation of viscoplastic behavior in heterogeneous polycrystals, Textures Microstruct. 11 (1989) 57–71.

[21] A. Molinari, G.R. Canova, S. Ahzi, A self consistent approach of the large deformation polycrystal viscoplasticity, Acta Metall. 35 (1987) 2983–2994.

[22] V. Sundararaghavan, N. Zabaras, Design of microstructure-sensitive properties in elasto-viscoplastic polycrystals using multi-scale homogenization, Int. J. Plast. 22 (2006) 1799–1824.

[23] V. Sundararaghavan, N. Zabaras, Linear analysis of texture-property relationships using process-based representations of Rodrigues space, Acta Mater. 55 (2007) 1573–1587.

[24] S. Sun, V. Sundararaghavan, A peridynamic implementation of crystal plasticity, Int. J. Solids Struct. 51 (2014) 3350–3360.

[25] V. Sundararaghavan, N. Zabaras, A multi-length scale continuum sensitivity analysis for the control of texture-dependent properties in deformation processing, Int. J. Plast. 24 (2008) 1581–1605.